Coseismic landslides reveal near-surface rock strength in a high-relief, tectonically active setting

Sean F. Gallen[1], Marin K. Clark[1], and Jonathan W. Godt[2]
[1]Department of Earth and Environmental Sciences, University of Michigan, Ann Arbor, Michigan 48109, USA
[2]Natural Hazards Mission Area, Landslide Hazards Program, U.S. Geological Survey, Denver, Colorado 80225, USA

ABSTRACT

We present quantitative estimates of near-surface rock strength relevant to landscape evolution and landslide hazard assessment for 15 geologic map units of the Longmen Shan, China. Strength estimates are derived from a novel method that inverts earthquake peak ground acceleration models and coseismic landslide inventories to obtain material properties and landslide thickness. Aggregate rock strength is determined by prescribing a friction angle of 30° and solving for effective cohesion. Effective cohesion ranges are from 70 kPa to 107 kPa for 15 geologic map units, and are approximately an order of magnitude less than typical laboratory measurements, probably because laboratory tests on hand-sized specimens do not incorporate the effects of heterogeneity and fracturing that likely control near-surface strength at the hillslope scale. We find that strength among the geologic map units studied varies by less than a factor of two. However, increased weakening of units with proximity to the range front, where precipitation and active fault density are the greatest, suggests that climatic and tectonic factors overwhelm lithologic differences in rock strength in this high-relief tectonically active setting.

INTRODUCTION

Large earthquakes in mountainous regions commonly result in catastrophic and widespread landsliding, which is a significant hazard during and in the immediate aftermath of ground shaking (Keefer, 1994). In recent years, unprecedented geomorphic data sets of large coseismic landsliding events have helped refine our understanding of the relationship between strong ground motion and mass wasting (Meunier et al., 2007, 2013; Hovius et al., 2011; Parker et al., 2011). With these developments, the opportunity exists to exploit large earthquakes and the consequent landscape response to quantify near-surface rock strength under dynamic conditions at the hillslope scale (10^3–10^6 m^2). From this perspective, the earthquake provides a regional shear-strength test where the earthquake imparts a measurable forcing (strong ground motion) and an observable response (slope failure) that is dependent on material strength.

The material strength of rock sets limits on topographic relief and modulates feedbacks between surface processes, tectonics, and climate (Schmidt and Montgomery, 1995; Burbank et al., 1996; Montgomery and Brandon, 2002). The strength of upper crustal earth materials generally is described using Mohr-Coulomb failure criteria, where shear strength is defined as the shear stress at failure, which is equal to the cohesion plus the product of the normal stress and the tangent of the angle of internal friction. Cohesion arises from the physical and chemical bonds in materials and friction describes the forces resisting motion between particles. The aggregate shear strength of soil or rock is described by the additive contributions of cohesive and frictional strength. Fractures, joints, and other discontinuities set the upper limit of rock strength, where their integrated effect acts to weaken rock at increasing spatial scales (Schmidt and Montgomery, 1995; Hoek and Brown, 1980). Thus, natural hillslope strength arises from the interplay of lithology, tectonic history, and climate.

Standard laboratory samples are too small to incorporate the scale and aggregate effect of strength-limiting discontinuities, and laboratory testing of large specimens that capture the true spatial heterogeneity of rock is not practical. These limitations have forced researchers to rely on qualitative measures to extrapolate laboratory measurements or use ranked classification schemes based on field observations to approximate rock strength at large spatial scales (Selby, 1980; Hoek and Brown, 1997). Although the Culmann (1875) criterion has been proposed as a way to estimate bedrock strength from hillslope height, this might apply only to deep-seated landsliding, and might not represent the integrated strength of the soil, regolith, and bedrock that characterizes many near-surface environments (Schmidt and Montgomery, 1995). Despite long recognition of these limitations, it remains notoriously difficult to quantify near-surface rock strength at geomorphically meaningful scales (Hoek and Brown, 1980, 1997), yet doing so is required to further our understanding of the role of rock strength in setting the pace of landscape evolution and to improve the accuracy of landslide hazard assessments.

Here we show how earthquake-triggered landslides and modeled peak ground acceleration (PGA) can be inverted to quantitatively document spatial trends in hillslope-scale rock strength using an example from the A.D. 2008 M_w 7.9 Wenchuan earthquake in Sichuan Province, China. The availability of high-resolution geologic and geomorphic data sets and geophysical models of seismic ground motion makes the Wenchuan earthquake the ideal natural laboratory to demonstrate the viability of using earthquake-triggered landslides to determine rock strength (Fig. 1). The earthquake occurred along the range front of the Longmen Shan and triggered >56,000 coseismic landslides over an

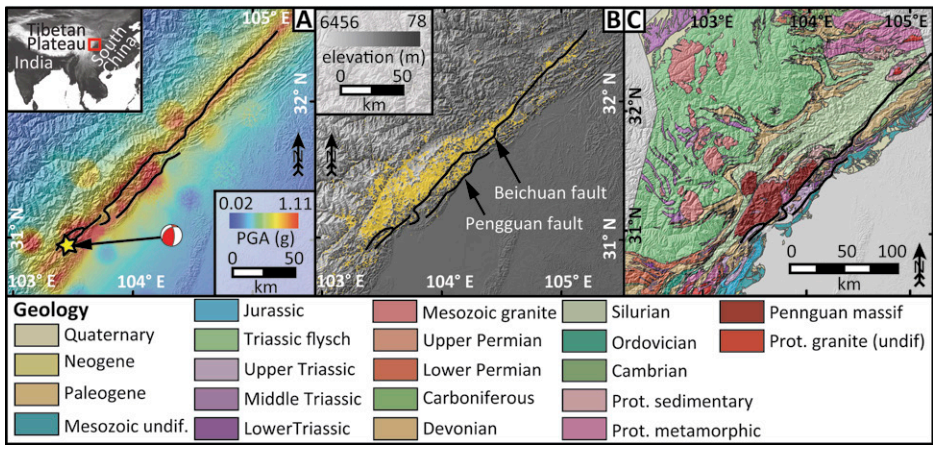

Figure 1. A: Shaded relief map of the Longmen Shan, Sichuan Provence, China, overlying a maximum peak ground acceleration (PGA) map (Worden et al., 2010) (undif.—undifferentiated; Prot.—Proterozoic). Yellow star indicates earthquake epicenter. B: Coseismic landslides (yellow) over shaded relief map (Dai et al., 2011). C: The traces of the Beichuan and Pengguan fault surface ruptures are shown as black bold lines in map adapted from 1:200,000-scale geologic maps (Ministry of Geology and Mineral Resources, 1991; Burchfiel et al., 1995).

area of >40,000 km^2 (Dai et al., 2011). Coseismic landslides occurred in an array of different rock types and topographic conditions affected by a range of ground accelerations (Fig. 1; Ministry of Geology and Mineral Resources, 1991; Burchfiel et al., 1995; Worden et al., 2010). These slope failures also contributed to a large number of fatalities, and have had long-lasting societal and ecological impacts as rivers slowly transport material from affected areas (Huang and Fan, 2013).

METHODS

We develop a mechanistic coseismic landslide model adapted from the Newmark (1965) sliding-block model commonly used for assessment of earthquake-induced landslide potential given a particular ground-shaking scenario (Wieczorek et al., 1985). The determination of strength parameters is relatively straightforward (Fig. DR1 in the GSA Data Repository[1]). Initial points of failure are identified in the digital elevation model (DEM) from the Newmark analysis, and depend on topographic slope and material properties; a synthetic landslide inventory is generated from these failure points using prescribed failure geometry. We perform a brute-force search to solve for the best-fit strength parameters that reproduce the frequency-area statistics of the mapped landslide inventory. In addition, we compare model results to total landslide volume and spatial distributions of landslide area and frequency as further model validation (for a full model description, see the Data Repository).

Prediction of hillslope failure is modeled using an infinite-slope stability analysis in which shear strength can be described using the angle of internal friction and cohesion. Coseismic surface displacements are calculated based on a critical (or yield) acceleration necessary to initiate displacement, from which material strength and topographic slope determine landslide susceptibility. Newmark displacements consider only rigid-block movements (i.e., no internal deformation) and plastic deformation at the base of the displaced mass. While other approaches consider internal deformation and elevated dynamic stresses that arise during movement, the Newmark analysis has been argued to be appropriate for regional-scale studies of coseismic landslides (Jibson et al., 2000; Godt et al., 2008).

Synthetic landslides are generated by first identifying target grid cells that exceed a threshold surface displacement (Newmark displacement of ≥5 cm) considering the critical acceleration necessary to initiate slope failure (Wieczorek et al., 1985; Jibson et al., 2000; Godt et al., 2008). Target cell displacements depend on local topographic slope (Shuttle Radar Topography mission DEM; ~90 m resolution) and material strength properties, which are calculated for each geologic map unit (age and lithology). We consider a range of reasonable material strength values for each geologic map unit based on the literature (Schmidt and Montgomery, 1995; Hoek and Brown, 1980, 1997; Jibson et al., 2000).

Comparison of grid-based simulations with an observed landslide inventory requires some scheme to aggregate the one-dimensional (1-D) slope-stability solution to determine landslide area and volume. We apply geometric criteria to predict landslide area and volume for each target cell; this effectively expands the 1-D approximation into a 3-D synthetic landslide inventory. We considered a suite of landslide geometries constrained by different topographic boundary conditions, such as slope of the target cell and upslope distance to the nearest divide (Fig. 2A). All landslide geometries are modeled to extend a failure plane upslope from the target cell, which excludes consideration of transport of material and run out; in this way failure of the target cell acts to destabilize upslope cells beneath a failure plane. This is analogous to undercutting a slope and is an approach similar to that used to model deep-seated bedrock failures (Densmore et al., 1998).

The power-law exponent of the modeled frequency-area statistics is sensitive to the choice of geometric criteria to define the 3-D geometry of the landslide (Figs. 2A and 2B). We find that the best-fit model considers a concave-upward failure plane (i.e., bowl shaped) that extends from the target cell upslope until it reaches the surface, matching not only the power-law exponent but also the total landslide volume (Figs. 2A and 2B). The advantage of this geometry is that we obtain landslide depths and volumes independent of empirical scaling relationships (Hovius et al., 1997; Larsen et al., 2010); this enables comparison of total model volume to that of the measured inventory volume.

The frequency-area power-law scaling constant is determined by material strength and landslide thickness (Fig. 2C). This finding provides a means to quantify hillslope-scale rock strength by using a brute-force search to find the strength parameters for each geologic map unit to minimize χ^2 (goodness-of-fit) between the observed and modeled landslide frequency-area distributions. Cohesion and thickness are treated as a ratio to avoid making a priori assumptions about landslide thickness.

Because the cohesion:thickness ratio and friction angle affect the power-law scaling constant similarly, no unique combination of these parameters minimizes χ^2 (Fig. DR2; see the Data Repository). We use a constant friction angle of 30° (approximately the average modal hillslope angle; Fig. DR3) and solve for an effective cohesion. While the actual partitioning of friction and cohesion may differ from our calculations, the aggregate rock strength determined from the combination of these terms is the same as natural rock strength. Thus, effective cohesion normalized to a fixed fiction angle reflects the true relative differences in total rock strength.

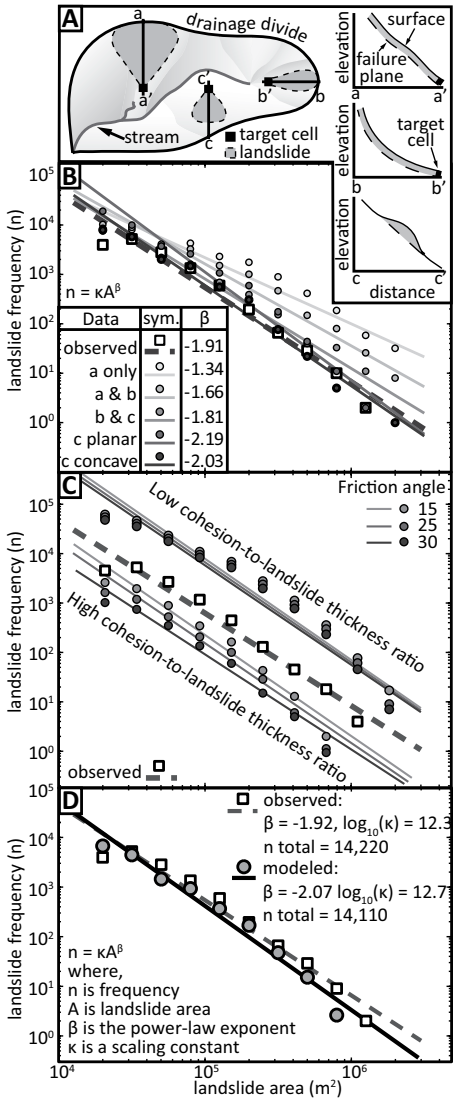

Figure 2. A: Different landslide geometries, each constrained by different topographic boundary conditions, considered in modeling. Four different models were tested, model a (a-a'), model b (b-b'), and model c (c-c') with either a planar (c planar) or concave (c concave) failure plane (for a full description, see the Data Repository [see footnote 1]). B: Influence of landslide geometries (letters in data column correspond to model descriptions in A) on statistical populations (sym.—symbol). Abbreviations as in D. C: Influence of strength parameters on modeled landslide statistics (using best-fit landslide geometry). B and C were run using regionally uniform strength parameters. D: Observed and best-fit modeled (determined from best-fit strength parameters for each geologic map unit) coseismic landslide inventories.

[1]GSA Data Repository item 2015016, Table DR1 and Figures DR1–DR7, is available online at www.geosociety.org/pubs/ft2015.htm, or on request from editing@geosociety.org or Documents Secretary, GSA, P.O. Box 9140, Boulder, CO 80301, USA.

RESULTS AND DISCUSSION

We find statistically meaningful fits for the 15 geologic map units that we use to model the regional distribution of coseismic landslides (Figs. 2D and 3). Mean effective cohesion varies between 70 and 107 kPa, within the bounds of values estimated for hillslope-scale strength (Schmidt and Montgomery, 1995), and is roughly an order of magnitude lower than typical laboratory measurements (Fig. 4A) (Hoek and Brown, 1980, 1997). When we set cohesion to zero and solve for a best-fit effective friction angle, the same relative pattern in rock strength is found, and mean (±1σ) values are 50° ± 4° (Fig. DR4). These friction angles would be considered high even for intact rock strength (Hoek and Brown, 1997), suggesting that cohesion is an important component of hillslope-scale strength. This finding challenges the notion that rock strength at large scales is almost entirely frictional (cf. Burbank et al., 1996; Korup, 2008).

Due to the resolution of the digital topography (~90 m) and PGA maps used in our study, we do not attempt to reproduce the extent and location of individual landslides; rather, our goal is to mimic drainage basin–scale to regional-scale statistics and spatial trends. The spatial pattern of our best-fit model matches the observed landslide inventory with mean misfits (±1σ) of 1.0% ± 10.2% and −3.6% ± 10.7% for landslide point and area densities, respectively (Fig. 3; Figs. DR5 and DR6). Principle component analysis shows that the model misfits exhibit no systematic correlation to the model inputs (Table DR1). Because we limit the observed inventory to the resolution of our model space (15,000–3,000,000 m^2), it is reasonable to assume that errors associated with poorly resolved, small landslides within the study area are minimized (e.g., Li et al., 2014). Model misfits are likely a result of preforming an inversion at a coarse resolution (individual geologic map units cover areas between ~400 and 22,000 km^2) that likely averages local variations in rock strength. In addition, the PGA map used in our inversion might underestimate ground motions in the northeastern potion of the fault rupture where displacements were largely strike slip (Shen et al., 2009), and it does not take into account topographic site effects that can amplify seismic waves and cause local peaks in PGA and landslide concentrations (Meunier et al., 2008).

Model mean landslide thickness ranges from 6.8 m to 8.6 m and the total landslide volume is ~4–7 km^3, on par with empirically derived estimates of 6–13 m depth and 3–7 km^3 volume estimated from the mapped inventory over the restricted model space (Fig. DR7) (Parker et al., 2011; Li et al., 2014; Larsen et al., 2010). The range of depths for observed and modeled landslides (one to tens of meters) indicates that failure occurred in a range of materials, from soil to weathered and fresh bedrock. We interpret our calculations as reflecting the strength of regolith and weathered or fractured bedrock that characterizes many near-surface environments (Anderson et al., 2013).

No obvious trend is observed between lithology and shear strength, implying that lithology plays little role in dictating the spatial variability of near-surface rock strength in the Longmen Shan (Fig. 4A). However, a positive correlation is noted between effective cohesion and distance from the range front (Figs. 4B and 4C). Both active fault density and the mean annual precipitation increase approaching the range front (Fig. 4D) (Burchfiel et al., 1995; Hijmans et al., 2005), so we speculate that in this humid, high-relief, tectonically active setting, tectonic and climatic history overwhelm intrinsic material properties and set limits on near-surface rock strength. If this inference is correct, reduced rock strength approaching the range front might be common in active orogenic belts owing to increased deformation toward the mountain front and the development of orographic precipitation, which would promote more rapid weathering and increase saturated conditions nearest the fault zone.

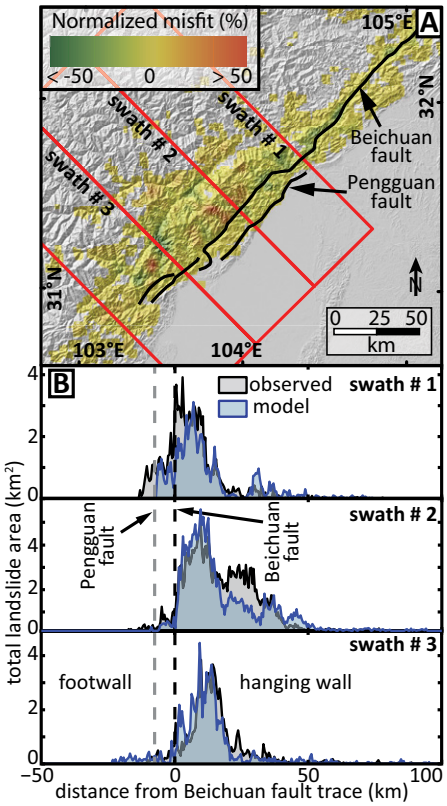

Figure 3. A: Map view of misfits between the modeled and observed landslide area densities per square kilometer, with locations of swath profiles (red boxes). B: Three ~50-km-wide swath profiles of landslide area densities. Supporting data are in Figures DR5 and DR6 (see footnote 1).

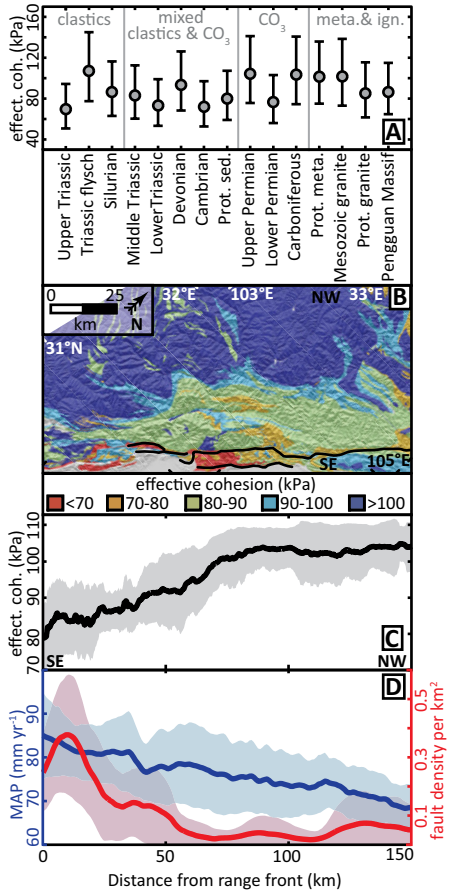

Figure 4. A: Effective cohesion (effect. coh.) with 1σ error bars determined from the standard derivation of mean landslide thickness for each geologic map unit (Fig. DR7; see footnote 1). The geologic map units are ordered by lithology (meta.—metamorphic; ign.—igneous; sed.—sedimentary; Prot.—Proterozoic.). B: Map view of mean effective cohesion for each geologic map unit. C, D: 300-km-wide swath profiles plotted as a function of distance from the range front. C: Mean effective cohesion (black line) and one standard error (gray area). D: Mean annual precipitation (MAP) derived from 3-arc second (~1 km) global data (Hijmans et al., 2005), and active fault density (Burchfiel et al., 1995). Lines and shaded areas show the mean and one standard error, respectively. Geologic map unit descriptions (Ministry of Geology and Mineral Resources, 1991; Burchfiel et al., 1995): Upper Triassic—siltstone, mudstone; Triassic flysch—mudstones and sandstones, low metamorphic grade; Silurian—mudstone, sandstone, marl; Middle Triassic—limestone, mudstone, local evaporites; Lower Triassic—limestone, marine clastics; Devonian—marine clastics, limestone; Cambrian—sandstone, evaporates, limestone; Proterozoic sedimentary—marine clastics, dolostone, limestone; upper and lower Permian—limestone, dolostone; Carboniferous—limestone; Proterozoic metamorphic—amphibolite-grade metasedimentary and metavolcanics; Mesozoic granite; Proterozoic granite; undifferentiated; Pengguan Massif—Proterozoic granite.

IMPLICATIONS

The low shear strength of rocks determined here underscores the difficulty of extrapolating laboratory strength tests to geomorphic problems. Because a single geotechnical measure or proxy is unlikely to fully capture the integrated strength at hillslope scales, we suggest that using extreme events that exert a large and measurable forcing on the landscape is a way forward to understand rock strength in the near-surface environment. We anticipate that rock strength, influenced by the effects of tectonic fracturing and climate, will quantitatively relate to erodibility because reduced rock strength suggests that the substrate is more easily detached and mobilized into the overlying soil column and available to transport by gravity, rivers, and glaciers (Molnar et al., 2007; Anderson et al., 2013). Advances in our ability to quantify hillslope-scale rock strength will also improve the implementation of landslide hazard models, thereby supporting efforts to reduce fatalities associated with seismically induced landslides.

ACKNOWLEDGMENTS

This work is supported by the University of Michigan Department of Earth and Environmental Sciences, Turner Postdoctoral Fellowship to Gallen; a visiting faculty CIRES (Cooperative Institute for Research in Environmental Sciences) fellowship from the University of Colorado to Clark; and in part through computational resources and services provided by Advanced Research Computing at the University of Michigan, Ann Arbor. We thank F.C. Dai for providing access to the landslide inventory used in this study, and Isaac Larsen, Randall Jibson, and two anonymous reviewers for comments that improved the manuscript.

REFERENCES CITED

Anderson, R.S., Anderson, S.P., and Tucker, G.E., 2013, Rock damage and regolith transport by frost: An example of climate modulation of the geomorphology of the critical zone: Earth Surface Processes and Landforms, v. 38, p. 299–316, doi:10.1002/esp.3330.

Burbank, D.W., Leland, J., Fielding, E., Anderson, R.S., Brozovic, N., Reid, M.R., and Duncan, C., 1996, Bedrock incision, rock uplift and threshold hillslopes in the northwestern Himalayas: Nature, v. 379, p. 505–510, doi:10.1038/379505a0.

Burchfiel, B., Chen, Z., Liu, Y., and Royden, L., 1995, Tectonics of the Longmen Shan and adjacent regions, central China: International Geology Review, v. 37, p. 661–735, doi:10.1080/00206819509465424.

Culmann, C., 1875, Die Graphische Statik: Zurich, Switzerland, Meyer and Zeller, 644 p.

Dai, F.C., Xu, C., Yao, X., Xu, L., Tu, X.B., and Gong, Q.M., 2011, Spatial distribution of landslides triggered by the 2008 Ms 8.0 Wenchuan earthquake, China: Journal of Asian Earth Sciences, v. 40, p. 883–895, doi:10.1016/j.jseaes.2010.04.010.

Densmore, A.L., Ellis, M.A., and Anderson, R.S., 1998, Landsliding and the evolution of normal-fault-bounded mountains: Journal of Geophysical Research, v. 103, p. 15203–15219, doi:10.1029/98JB00510.

Godt, J.W., Şener, B., Verdin, K.L., Wald, D.J., Earle, P.S., Harp, E.L., and Jibson, R.W., 2008, Rapid assessment of earthquake-induced landsliding, *in* Proceedings of the First World Landslide Forum, 18-21 November 2008, Tokyo, Japan: Global Promotion Committee of the International Programme on Landslides, p. 219–222.

Hijmans, R.J., Cameron, S.E., Parra, J.L., Jones, P.G., and Jarvis, A., 2005, Very high resolution interpolated climate surfaces for global land areas: International Journal of Climatology, v. 25, p. 1965–1978, doi:10.1002/joc.1276.

Hoek, E., and Brown, E. T., 1980, Empirical strength criterion for rock masses: Journal of Geotechnical and Geoenvironmental Engineering, v. 106, p. 1013–1035.

Hoek, E., and Brown, E.T., 1997, Practical estimates of rock mass strength: International Journal of Rock Mechanics and Mining Sciences, v. 34, p. 1165–1186, doi:10.1016/S1365-1609(97)80069-X.

Hovius, N., Stark, C.P., and Allen, P.A., 1997, Sediment flux from a mountain belt derived by landslide mapping: Geology, v. 25, p. 231–234, doi:10.1130/0091-7613(1997)025<0231:SFFAMB>2.3.CO;2.

Hovius, N., Meunier, P., Lin, C.-W., Chen, H., Chen, Y.-G., Dadson, S., Horng, M.-J., and Lines, M., 2011, Prolonged seismically induced erosion and the mass balance of a large earthquake: Earth and Planetary Science Letters, v. 304, p. 347–355, doi:10.1016/j.epsl.2011.02.005.

Huang, R., and Fan, X., 2013, The landslide story: Nature Geoscience, v. 6, p. 325–326, doi:10.1038/ngeo1806.

Jibson, R.W., Harp, E.L., and Michael, J.A., 2000, A method for producing digital probabilistic seismic landslide hazard maps: Engineering Geology, v. 58, p. 271–289, doi:10.1016/S0013-7952(00)00039-9.

Keefer, D.K., 1994, The importance of earthquake-induced landslides to long-term slope erosion and slope-failure hazards in seismically active regions: Geomorphology, v. 10, p. 265–284, doi:10.1016/0169-555X(94)90021-3.

Korup, O., 2008, Rock type leaves topographic signature in landslide-dominated mountain ranges: Geophysical Research Letters, v. 35, L11402, doi:10.1029/2008GL034157.

Larsen, I.J., Montgomery, D.R., and Korup, O., 2010, Landslide erosion controlled by hillslope material: Nature Geoscience, v. 3, p. 247–251, doi:10.1038/ngeo776.

Li, G., West, A.J., Densmore, A.L., Jin, Z., Parker, R.N., and Hilton, R.G., 2014, Seismic mountain building: Landslides associated with the 2008 Wenchuan earthquake in the context of a generalized model for earthquake volume balance: Geochemistry Geophysics Geosystems, v. 15, p. 833–844, doi:10.1002/2013GC005067.

Meunier, P., Hovius, N., and Haines, A.J., 2007, Regional patterns of earthquake-triggered landslides and their relation to ground motion: Geophysical Research Letters, v. 34, L20408, doi:10.1029/2007GL031337.

Meunier, P., Hovius, N., and Haines, J.A., 2008, Topographic site effects and the location of earthquake induced landslides: Earth and Planetary Science Letters, v. 275, p. 221–232, doi:10.1016/j.epsl.2008.07.020.

Meunier, P., Uchida, T., and Hovius, N., 2013, Landslide patterns reveal the sources of large earthquakes: Earth and Planetary Science Letters, v. 363, p. 27–33, doi:10.1016/j.epsl.2012.12.018.

Ministry of Geology and Mineral Resources, 1991, Regional geology of Sichuan Province: Beijing, Geological Publishing House, 728 p. (in Chinese)

Molnar, P., Anderson, R.S., and Anderson, S.P., 2007, Tectonics, fracturing of rock, and erosion: Journal of Geophysical Research, v. 112, F03014, doi:10.1029/2005JF000433.

Montgomery, D.R., and Brandon, M.T., 2002, Topographic controls on erosion rates in tectonically active mountain ranges: Earth and Planetary Science Letters, v. 201, p. 481–489, doi:10.1016/S0012-821X(02)00725-2.

Newmark, N.M., 1965, Effects of earthquakes on dams and embankments: Geotechnique, v. 15, p. 139–160, doi:10.1680/geot.1965.15.2.139.

Parker, R.N., Densmore, A.L., Rosser, N.J., de Michele, M., Li, Y., Huang, R., Whadcoat, S., and Petley, D.N., 2011, Mass wasting triggered by the 2008 Wenchuan earthquake is greater than orogenic growth: Nature Geoscience, v. 4, p. 449–452, doi:10.1038/ngeo1154.

Schmidt, K.M., and Montgomery, D.R., 1995, Limits to relief: Science, v. 270, p. 617–620, doi:10.1126/science.270.5236.617.

Selby, M.J., 1980, A rock mass strength classification for geomorphic purposes: With tests from Antarctica and New Zealand: Zeitschrift für Geomorphologie, v. 24, p. 31–51.

Shen, Z.K., Sun, J., Zhang, P., Wan, Y., Wang, M., Bürgmann, R., Zeng, Y., Gan, W., Hiao, H., and Wang, Q., 2009, Slip maxima at fault junctions and rupturing of bariers during the 2008 Wenchuan earthquake: Nature Geoscience, v. 2, p. 718–724, doi:10.1038/NGEO636.

Wieczorek, G.F., Wilson, R.C., and Harp, E.L., 1985, Map showing slope stability during earthquakes in San Mateo County, California: U.S. Geological Survey Miscellaneous Investigations Map I-1257-E, scale 1:62,500.

Worden, C.B., Wald, D.J., Lin, K., Cua, G., and Garcia, D., 2010, A revised ground-motion and intensity interpolation scheme for ShakeMap: Seismological Society of America Bulletin, v. 100, p. 3083–3096, doi:10.1785/0120100101.

Manuscript received 15 July 2014
Revised manuscript received 3 October 2014
Manuscript accepted 8 October 2014

Printed in USA

ERRATUM

Coseismic landslides reveal near-surface rock strength in a high-relief tectonically active setting

S.F. Gallen, M.K. Clark, and J.W. Godt
Geology v. 43, p. 11–14, doi:10.1130/G36080.1

This erratum is to acknowledge the most up-to-date reference for the landslide inventory data used in this manuscript. In addition to Dai et al. (2011), the landslide inventory used was refined and expanded by Xu et al. (2014).

We would like to thank Chong Xu for noting this discrepancy and acknowledge Chong Xu and F.C. Dai for providing access to the landslide inventory.

REFERENCES:

Dai, F.C., Xu, C., Yao, X., Xu, L., Tu, X.B., and Gong, Q.M., 2011, Spatial distribution of landslides triggered by the 2008 M_s 8.0 Wenchuan earthquake, China: Journal of Asian Earth Sciences, v. 40, p. 883–895, doi:10.1016/j.jseaes.2010.04.010.

Xu, C., Xu, X., Yao, X., and Dai, F., 2014, Three (nearly) complete inventories of landslides triggered by the May 12, 2008 Wenchuan M_w 7.9 earthquake of China and their spatial distribution statistical analysis: Landslides, v. 11, p. 441–461, doi:10.1007/s10346-013-0404-6.